

# RC-GeoCP: Geometric Consensus for Radar-Camera Collaborative Perception

Xiaokai Bai<sup>1</sup>, Lianqing Zheng<sup>2</sup>, Runwei Guan<sup>3</sup>, Siyuan Cao<sup>1</sup>,  
and Huiliang Shen<sup>1</sup>

<sup>1</sup> College of Information Science and Electronic Engineering, Zhejiang University

<sup>2</sup> School of Automotive Studies, Tongji University

<sup>3</sup> Thrust of Artificial Intelligence, Hong Kong University of Science and Technology,  
shawnnkb@gmail.com

**Abstract.** Collaborative perception (CP) enhances scene understanding through multi-agent information sharing. While LiDAR-centric systems offer precise geometry, high costs and performance degradation in adverse weather necessitate multi-modal alternatives. Despite dense visual semantics and robust spatial measurements, the synergy between cameras and 4D radar remains underexplored in collaborative settings. This work introduces RC-GeoCP, the first framework to explore the fusion of 4D radar and images in CP. To resolve misalignment caused by depth ambiguity and spatial dispersion across agents, RC-GeoCP establishes a radar-anchored geometric consensus. Specifically, Geometric Structure Rectification (GSR) aligns visual semantics with geometry derived from radar to generate spatially grounded, geometry-consistent representations. Uncertainty-Aware Communication (UAC) formulates selective transmission as a conditional entropy reduction process to prioritize informative features based on inter-agent disagreement. Finally, the Consensus-Driven Assembler (CDA) aggregates multi-agent information via shared geometric anchors to form a globally coherent representation. We establish the first unified radar-camera CP benchmark on V2X-Radar and V2X-R, demonstrating state-of-the-art performance with significantly reduced communication overhead. Code will be released soon.

**Keywords:** 4D Radar · Collaborative Perception · Multi-modal Fusion

## 1 Introduction

Collaborative perception (CP) aims to extend the sensing range and reliability of autonomous driving systems by sharing information among multiple agents, including vehicles and roadside infrastructure [46, 48, 52]. By enabling agents to access observations beyond their individual line-of-sight, CP provides a robust mechanism to overcome fundamental challenges such as long-range blind spots and severe occlusions [18, 39, 58]. Consequently, CP has evolved into a prominent research area, with substantial progress made in intermediate feature sharing [6, 47], communication efficiency [11, 12, 51], and multi-agent fusion [37, 42, 45].

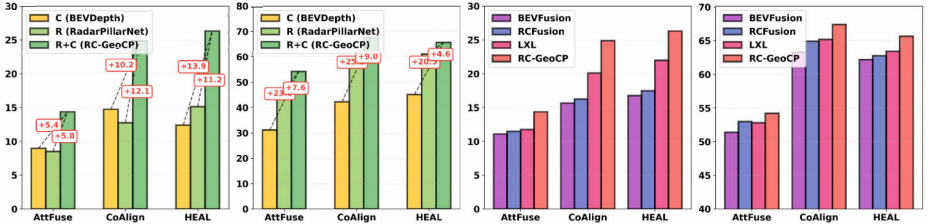


**Fig. 1:** Performance comparison on V2X-Radar (column 1,3) and V2X-R (column 2,4). As presented in column 1, 2, R+C fusion significantly outperforms single-modality baselines. Column 3, 4 show that our proposed RC-GeoCP consistently surpasses comparable radar-camera fusion methods across various collaborative perception frameworks.

Most existing CP frameworks are predominantly LiDAR-centric [11, 22, 47]. These methods typically exchange LiDAR point clouds or compressed features, leveraging the precise 3D geometry provided by LiDAR to facilitate spatial alignment and feature-level consensus [6, 9, 49]. While the strong geometric consistency of LiDAR has driven significant improvements in collaborative detection and tracking [10, 18, 39], its practical deployment is often constrained by high sensor costs and performance degradation in adverse weather conditions [7, 54]. This motivates the development of alternative sensing configurations, particularly multi-modal collaborative paradigms.

To address these challenges, multi-modal collaborative perception has gained increasing attention, particularly camera–radar configurations. Cameras provide dense visual observations and rich semantics for object recognition and scene understanding [20, 28, 40]. However, camera-only perception is sensitive to environmental conditions and viewpoint changes [19, 30]. Moreover, monocular features suffer from inherent depth ambiguity, causing spatial smearing along the optical ray during BEV projection [19, 31]. In collaborative settings, such ambiguity is amplified across agents, leading to geometric misalignment and degraded structural consistency [38, 42, 45]. In contrast, radar sensing offers complementary advantages [13, 50]. Millimeter-wave radar provides reliable range and velocity measurements and remains robust under adverse lighting and weather [8, 29, 32]. Importantly, radar observations are physically grounded and remain structurally consistent across viewpoints [14, 43]. While recent radar-based CP methods leverage these properties to enhance robustness [13, 51], radar signals are sparse and lack rich semantics, making them insufficient when used alone.

Taken together, these observations highlight the necessity of a principled integration of camera and radar in collaborative perception. While cameras contribute rich semantics, they lack spatial certainty; conversely, radar provides a stable, perspective-invariant spatial reference but with limited semantic detail [14, 19, 44]. Integrating these modalities is therefore essential to support robust and scalable CP under practical deployment constraints [5, 51, 53].

In this work, we propose RC-GeoCP, a framework that explores radar-camera collaborative perception through geometry-guided consensus. Our core idea is to leverage radar-derived geometric structure as a shared physical reference to anchor camera semantics. RC-GeoCP consists of three tightly coupled compo-

nents. First, Geometric Structure Rectification (GSR) aligns camera features to the radar frame and leverages radar attributes to guide deformable aggregation. This mechanism effectively constrains the spatial support of visual semantics to concrete geometric entities, mitigating the diffusion induced by depth ambiguity. Second, Uncertainty-Aware Communication (UAC) dynamically evaluates the epistemic uncertainty and spatial disagreement between ego and neighbor representations selectively retrieve high-value tokens to either enhance existing evidence or fill perceptual vacuums. It selectively retrieves informative tokens from neighbors that either reinforce existing evidence or compensate for the ego-vehicle’s perceptual gaps, ensuring bandwidth efficiency [23, 33, 53]. Finally, a Consensus Driven Assembler (CDA) utilizes radar-derived global geometric consensus as physical addresses, which are injected into attention mechanism to assemble heterogeneous tokens from multiple agents, which produces a structurally coherent representation for collaborative perception [9, 27, 34].

We evaluate RC-GeoCP on the V2X-Radar [50] and V2X-R [13] datasets, marking one of the first unified evaluations of radar-camera collaborative perception (CP). As presented in Figure 1, experimental results demonstrate that RC-GeoCP achieves state-of-the-art performance with reduced communication overhead, validating the effectiveness of geometric consensus in multi-modal collaboration. Our contributions are summarized as follows:

- We propose RC-GeoCP, a novel radar–camera CP framework that establishes geometric consensus to guide both communication selection and multi-agent fusion, achieving performance–bandwidth trade-offs.
- We introduce GSR to rectify diffuse visual features and transform them into spatially grounded representations using radar physical cues.
- We develop UAC and CDA to manage demand-driven communication and structurally coherent aggregation through shared geometric anchors.
- We establish radar–camera CP benchmarks on V2X-Radar and V2X-R, providing a solid foundation for future research in robust multi-agent perception.

## 2 Related Work

### 2.1 Collaborative Perception

Research in collaborative perception has evolved from early fusion of raw sensor data to more bandwidth-efficient intermediate fusion strategies. Pioneering frameworks such as V2VNet [39] and V2X-ViT [47] utilize Graph Neural Networks (GNNs) and Vision Transformers to aggregate compressed feature maps from neighboring agents. While these methods demonstrate significant performance gains over single-agent baselines, they primarily focus on homogeneous LiDAR-based settings and often assume ideal communication channels. To address real-world bandwidth limitations, sparse communication strategies have gained prominence. Where2comm [11] introduces spatial confidence maps to transmit only perceptually critical regions, while SlimComm [51] and other query-based approaches [45] leverage semantic priors to guide feature selection.

However, these methods typically optimize what to send based on scalar confidence values, often overlooking the geometric consistency of the transmitted features. In camera-based systems, sparse transmission can exacerbate feature misalignment due to the lack of explicit depth information. Recent works like CoAlign [27] and TraF-Align [35] attempt to correct pose errors and temporal latency through graph optimization and trajectory prediction, yet they remain susceptible to the spatial smearing inherent in vision-only features. In this work, we advance this domain by incorporating a uncertainty-aware selection mechanism that targets high-entropy regions where local observations conflict, ensuring that bandwidth is allocated to resolving geometric ambiguity rather than merely reinforcing high-confidence redundancy.

## 2.2 Radar-based Perception

The utilization of radar in autonomous driving has traditionally been limited to low-resolution object tracking. However, the advent of 4D imaging radar has spurred a new wave of research in multi-modal fusion [1–4, 17, 41, 56, 57]. In single-agent settings, methods such as CenterFusion [29] and CRAFT [14] associate radar points with image frustums to improve 3D detection. More recently, Bird’s-Eye-View (BEV) fusion architectures like CRN [15], LXL [43], and RCBEVDet [21] have set new benchmarks by using radar occupancy grids to guide the Lift-Splat-Shoot (LSS) [31] view transformation. These approaches utilize radar to correct the ill-posed depth estimation of monocular cameras, effectively sculpting the 3D feature volume to match physical occupancy.

Despite these advancements, the application of radar-camera fusion in collaborative perception remains underexplored due to the lack of suitable datasets and the complexity of aligning asynchronous radar frames across agents. Existing multi-modal CP works often treat radar as a auxiliary modality for robustness [13, 51]. In contrast, RC-GeoCP adapts the principles of radar-guided view transformation to the V2X context, establishing radar as the geometric anchor to enforce consensus among spatially disjoint and semantically diffuse visual observations. This work establishes the first unified radar-camera collaborative perception benchmark on V2X-Radar and V2X-R, providing a foundation for robust multi-agent research.

## 3 Method

RC-GeoCP aims to resolve the geometric inconsistency of camera features in collaborative perception by establishing a radar-anchored geometric consensus shared across agents. Given a set of connected agents equipped with cameras and 4D radars, RC-GeoCP constructs a geometry-driven collaboration pipeline that aligns visual semantics to physical space (GSR in Section 3.3), selectively communicates high-value information (in Section 3.4), and aggregates multi-agent evidence through shared geometric anchors (CDA in Section 3.5).

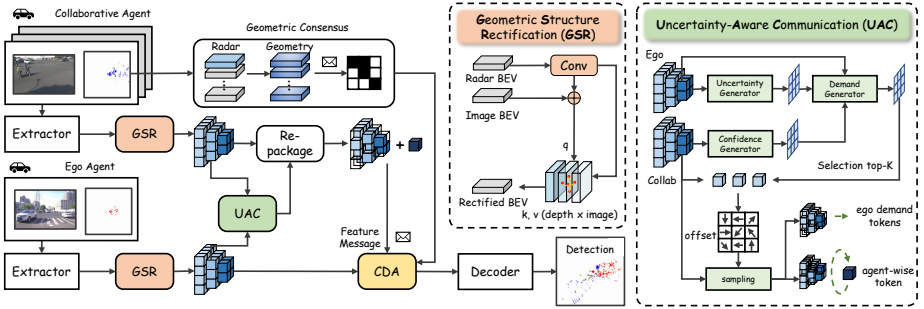


**Fig. 2:** Overview of RC-GeoCP. First, Geometric Structure Rectification (GSR) addresses visual feature dispersion by aligning camera-derived semantics with radar-based spatial cues. Then, Uncertainty-Aware Communication (UAC) selects informative tokens and repackages them for efficient transmission. Finally, Consensus-Driven Aggregation (CDA) combines data from multiple agents by leveraging radar-derived geometric consensus, ensuring spatially consistent multi-modal collaborative perception.

### 3.1 Problem Formulation

Consider a collaborative perception system consisting of  $N$  connected agents. Each agent  $i \in \{1, \dots, N\}$  is equipped with multi-view cameras and a 4D radar sensor, producing local observations  $\mathcal{O}_i = \{\mathcal{I}_i, \mathcal{R}_i\}$ , where  $\mathcal{I}_i$  and  $\mathcal{R}_i$  denote camera images and radar measurements, respectively. Based on these observations, agent  $i$  extracts a local BEV feature  $\mathbf{F}_i \in \mathbb{R}^{C \times H \times W}$  in its own coordinate frame, where  $C$  is feature channel while  $(H, W)$  denotes BEV resolution.

In collaborative perception, an ego agent  $i$  aggregates its own BEV feature together with messages  $\{\mathbf{P}_{j \rightarrow i}\}_{j \in \mathcal{N}(i)}$  received from neighboring agents to perform downstream 3D perception tasks. This process is modeled as

$$\mathbf{F}_i^{\text{collab}} = \Phi_{\theta}(\mathbf{F}_i, \{\mathbf{P}_{j \rightarrow i}\}_{j \in \mathcal{N}(i)}), \quad (1)$$

where  $\Phi_{\theta}$  denotes the CP model. The objective is to maximize collaborative perception performance under a communication budget constraint:

$$\max_{\theta} \sum_{i=1}^N g(\mathbf{F}_i^{\text{collab}}, y_i), \quad \text{s.t.} \quad \sum_{j \in \mathcal{N}(i)} |\mathbf{P}_{j \rightarrow i}| \leq B_{\text{comm}}, \quad (2)$$

where  $y_i$  is the ground-truth supervision of agent  $i$ ,  $g(\cdot, \cdot)$  denotes task metric, and  $B_{\text{comm}}$  is the communication budget.

### 3.2 Overview of RC-GeoCP

Figure 2 illustrates the overall framework. Given local observations  $\mathcal{O}_i = \{\mathcal{I}_i, \mathcal{R}_i\}$ , each agent extracts camera and radar BEV features  $\mathbf{F}_i^{\text{cam}}$  and  $\mathbf{F}_i^{\text{rad}}$ .

(1) To mitigate viewpoint-dependent dispersion, camera BEV features are rectified by radar-derived geometry, i.e.,  $\tilde{\mathbf{F}}_i = \mathcal{R}(\mathbf{F}_i^{\text{cam}} | \mathbf{F}_i^{\text{rad}})$ , ensuring spatially consistent multi-modal collaborative perception.

(2) Under bandwidth constraints, each neighboring agent  $j$  selects a sparse set of tokens using an uncertainty-aware demand map  $\mathbf{W}_{i,j}$ , formulated as  $\mathbf{S}_{j \rightarrow i} = \mathcal{S}(\tilde{\mathbf{F}}_j | \mathbf{W}_{i,j})$ , which reflects the ego’s demand for complementary information.

(3) Finally, the ego agent aggregates the received tokens using a consensus-driven operator, expressed as  $\mathbf{F}_i^{\text{collab}} = \mathcal{A}(\tilde{\mathbf{F}}_i, \{\mathbf{S}_{j \rightarrow i}\} | \{\mathbf{W}_{i,j}, \mathbf{G}_{j \rightarrow i}^{\text{rad}}\})$ , where  $\mathbf{G}_{j \rightarrow i}^{\text{rad}}$  represents the geometric consensus for each agent.

### 3.3 Geometric Structure Rectification

Collaborative perception requires cross-agent geometric consistency. Conventional Lift-Splat-Shoot (LSS) paradigms often suffer from depth-semantic diffusion, where monocular uncertainty smears semantics along the depth axis, causing spatial misalignment. We propose Geometric Structure Rectification to ground camera semantics using sparse 4D radar cues as physical anchors.

We initialize the radar-grounded query field as  $\mathbf{Q}_i = \mathbf{F}_i^{\text{cam}} + \Phi_{\text{init}}(\mathcal{D}(\mathbf{F}_i^{\text{rad}}))$ , where  $\mathcal{D}(\cdot)$  is downsampling and  $\Phi_{\text{init}}$  is a zero-initialized convolutional layer. Deformable cross-attention then aggregates multi-view image features  $\mathbf{F}_i^{\text{img}}$  by lifting BEV queries into vertical pillars and projecting reference points  $q$  into image space. The rectified representation  $\mathbf{F}_i^{\text{rect}}$  is:

$$\mathbf{F}_i^{\text{rect}}(q) = \sum_{n=1}^N \mathbf{K}_n \mathbf{B} \cdot \phi(\mathbf{F}^{3\text{D}}, \mathcal{P}(q) + \Delta q_n), \quad (3)$$

where  $\Delta q_n$  are offsets conditioned on  $\mathbf{Q}_i$ , and  $\mathbf{F}^{3\text{D}}$  is the feature space constructed from image features and depth probabilities.

Finally, adaptive gated calibration balances visual richness with geometric precision. Crucially, radar acts as a guide rather than a decider. The gating mechanism attenuates radar influence when uncertainty is high to preserve the baseline performance of pure camera semantics. The final rectified feature  $\tilde{\mathbf{F}}_i$  is

$$\tilde{\mathbf{F}}_i = \mathbf{F}_i^{\text{rect}} + \sigma(\mathcal{G}(\mathbf{F}_i^{\text{rect}})) \odot \Psi(\mathbf{F}_i^{\text{rad}}), \quad (4)$$

where  $\sigma$  is sigmoid and  $\mathcal{G}$  is a gating convolution. This ensures radar geometry guides the representation primarily in regions of high visual uncertainty.

### 3.4 Uncertainty-Aware Communication

Collaborative perception requires identifying information that is both reliable and complementary under bandwidth constraints. Unlike heuristic methods, we formulate Uncertainty-Aware Communication (UAC) as an ego-centric conditional entropy reduction process. By dynamically evaluating epistemic uncertainty and inter-agent disagreement, RC-GeoCP strategically allocates bandwidth to resolve geometric ambiguities rather than reinforcing redundancy. This demand-driven mechanism ensures transmitted tokens effectively fill perceptual vacuums while maintaining high communication efficiency.

Given rectified features  $\tilde{\mathbf{F}}_i \in \mathbb{R}^{C \times H \times W}$ , a multi-scale BEV pyramid  $\{\tilde{\mathbf{F}}_i^{(l)}\}_{l=1}^L$  is constructed to support scale-adaptive communication. For each neighboring

agent  $j$ , RC-GeoCP avoids transmitting dense BEV features. Instead, only selected ego demand tokens and learnable agent-wise token are transmitted.

**Selected Ego Demand Tokens.** Specifically, each agent first predicts a semantic confidence map in its local coordinate frame and aligns it to the ego

$$\mathbf{C}_{j \rightarrow i}^{(l)} = \mathcal{T}_{j \rightarrow i} \left( \sigma \left( \Phi_{\text{conf}}^{(l)} \left( \tilde{\mathbf{F}}_j^{(l)} \right) \right) \right), \quad (5)$$

which reflects the reliability of agent  $j$ 's local perception. Here,  $\mathcal{T}_{j \rightarrow i}$  denotes transmission communication process from agent  $j$  to agent  $i$ . Only  $\mathbf{C}_{j \rightarrow i}^{(l)}$  is transmitted to support uncertainty-aware collaboration under bandwidth constraints. The ego agent estimates its own perceptual uncertainty as  $\mathbf{U}_i^{(l)} = 1 - \mathbf{C}_i^{(l)}$ , which highlights regions where additional information from neighbors is most needed.

To identify complementary evidence, RC-GeoCP models inter-agent perceptual disagreement  $\mathbf{D}_{i,j}^{(l)}$  as a conditional function of ego semantics and neighbor confidence through convolutional layer  $\Phi_{\text{diff}}^{(l)}$  as  $\mathbf{D}_{i,j}^{(l)} = \Phi_{\text{diff}}^{(l)}(\tilde{\mathbf{F}}_i^{(l)} \mid \mathbf{U}_i^{(l)}, \mathbf{C}_{j \rightarrow i}^{(l)})$ , where higher values indicate regions in which agent  $j$  provides information that deviates from the ego perception and is therefore potentially informative. Based on this disagreement signal, the ego infers a demand weight for each neighbor

$$\mathbf{W}_{i,j}^{(l)} = \frac{\sigma \left( \Phi_{\text{trust}}^{(l)} \left( \tilde{\mathbf{F}}_i^{(l)} \mid \mathbf{D}_{i,j}^{(l)} \right) \right)}{\sum_{k \in \{i\} \cup \mathcal{N}(i)} \sigma \left( \Phi_{\text{trust}}^{(l)} \left( \tilde{\mathbf{F}}_i^{(l)} \mid \mathbf{D}_{i,k}^{(l)} \right) \right) + \epsilon}, \quad (6)$$

which represents the ego-centric demand in the information provided by agent  $j$ , normalized across all participating agents.  $\Phi_{\text{trust}}^{(l)}$  is stacked convolutional layer.

Under bandwidth constraints, RC-GeoCP performs communication at the level of sparse tokens rather than dense feature maps. At each scale  $l$ , let  $\Lambda^{(l)} = \{1, \dots, H^{(l)}\} \times \{1, \dots, W^{(l)}\}$  denote the BEV grid index set, and  $\mathbf{W}_{i,j}^{(l)} \in (0, 1)^{H^{(l)} \times W^{(l)}}$  be the uncertainty-aware demand map that the ego agent infers for neighbor  $j$ . We select a subset of informative token locations  $\Omega_{i,j}^{(l)} \subseteq \Lambda^{(l)}$  via top- $K$  filtering, which can be formulated as

$$\Omega_{i,j}^{(l)} = \text{TopK} \left( \mathbf{W}_{i,j}^{(l)}, K^{(l)} \right), \quad (7)$$

where  $K^{(l)} = \lceil \rho^{(l)} \cdot |\Lambda^{(l)}| \rceil$ ,  $\rho^{(l)} \in (0, 1]$  is the token ratio controlling the communication budget at scale  $l$ , and  $|\Lambda^{(l)}| = H^{(l)}W^{(l)}$ .

Before transmission, RC-GeoCP refines only the selected tokens in the local coordinate frame of agent  $j$  to better capture complementary geometric and semantic context. A deformable refinement operator  $\mathcal{D}^{(l)}(\cdot)$  is applied to perform content-adaptive sampling around each selected location  $p \in \Omega_{i,j}^{(l)}$ , formulated as

$$\tilde{\mathbf{F}}_j^{(l)}(p) = \mathcal{D}^{(l)} \left( \tilde{\mathbf{F}}_j^{(l)}, p \right) + \tilde{\mathbf{F}}_j^{(l)}(p) \quad (8)$$

where  $\mathcal{D}^{(l)}(\cdot)$  denotes a deformable attention that aggregates local evidence with learned offsets, and residual preserves the original representation for stability.

**Table 1:** Comparison of collaborative perception performance on the validation/test sets of V2X-Radar [50] dataset and validation set of V2X-R [13] dataset. We implement all approaches under multi-modal setting.

Method	V2X-Radar Val. $\uparrow$		V2X-Radar Test $\uparrow$		V2X-R Val. $\uparrow$		Comm.
	AP@0.5	AP@0.7	AP@0.5	AP@0.7	AP@0.5	AP@0.7	
Who2com (ICRA2020) [23]	27.10	10.35	17.51	4.28	77.73	45.57	4.00
AttFuse (ICRA2022) [48]	33.01	11.09	24.78	5.75	76.76	51.39	4.00
AdaFusion (WACV2023) [16]	31.33	13.06	22.92	6.78	73.65	43.55	4.00
V2VNet (ECCV2020) [39]	36.37	14.58	30.28	8.25	77.21	48.44	4.00
CoAlign (ICRA2023) [27]	37.14	15.65	29.40	12.11	77.21	61.30	7.00
CoBEVT (CoRL2023) [45]	36.89	16.06	31.90	10.73	78.71	51.48	4.00
HEAL (ICLR2024) [26]	38.61	16.76	27.80	10.10	79.54	62.19	7.08
Where2comm (NIPS2022) [11]	40.83	17.92	33.19	11.10	75.64	44.60	4.00
V2XViT (ECCV2022) [47]	39.88	18.31	34.81	12.35	78.21	47.72	4.00
RC-GeoCP (ours)	44.55	25.92	42.61	18.77	81.90	65.09	2.39

**Learnable Agent-wise Token.** To compensate for the information discarded during sparse top- $k$  selection, we introduce multi-scale agent-wise tokens to aggregate the residual features. For each neighboring agent  $j$  at scale  $l$ , let  $\Omega_{i,j}^{(l)}$  denote the selected token indices. The remaining features are defined as  $\tilde{\mathbf{F}}_j^{(l),\text{res}} = \left\{ \tilde{\mathbf{F}}_j^{(l)}(p) \mid p \notin \Omega_{i,j}^{(l)} \right\}$ . A learnable agent token  $\mathbf{a}_j^{(l)}$  is used to aggregate these residual features via multi-head cross attention, which can be expressed as

$$\mathbf{e}_j^{(l)} = \text{Attn} \left( \mathbf{a}_j^{(l)}, \tilde{\mathbf{F}}_j^{(l),\text{res}}, \tilde{\mathbf{F}}_j^{(l),\text{res}} \right). \quad (9)$$

The compact embedding  $\mathbf{e}_j^{(l)}$  captures complementary information beyond selected tokens, ensuring global context preservation under sparse communication.

After local refinement, each neighboring agent transmits both the selected ego-demand tokens and the agent-wise token to the ego frame, defined as

$$\mathbf{S}_{j \rightarrow i}^{(l)} = \mathcal{T}_{j \rightarrow i} \left( \left\{ \tilde{\mathbf{F}}_j^{(l)}(p) \mid p \in \Omega_{i,j}^{(l)} \right\} \cup \left\{ \mathbf{e}_j^{(l)} \right\} \right), \quad (10)$$

where  $\mathbf{S}_{j \rightarrow i}^{(l)}$  denotes the communicated token set from agent  $j$  to the ego. The ego retains its full BEV representation, while neighboring agents transmit only sparse, demand-driven tokens together with a compact agent-level embedding. This design ensures bandwidth-efficient communication while preserving complementary context beyond selected regions.

Beyond token selection, ego demand map supervise collaborative consistency by aggregating confidence logits into a shared occupancy map, promoting agreement among reliable agents during training. This design enables uncertainty-aware communication that is both bandwidth-efficient and tightly coupled with downstream fusion. Details are deferred to the appendix.

### 3.5 Consensus-Driven Assembler

While Uncertainty-Aware Communication (UAC) identifies informative BEV tokens (selected ego demand tokens) and preserves complementary context via learnable agent-wise tokens, robust collaborative perception further requires enforcing geometric consistency during multi-agent aggregation. RC-GeoCP achieves

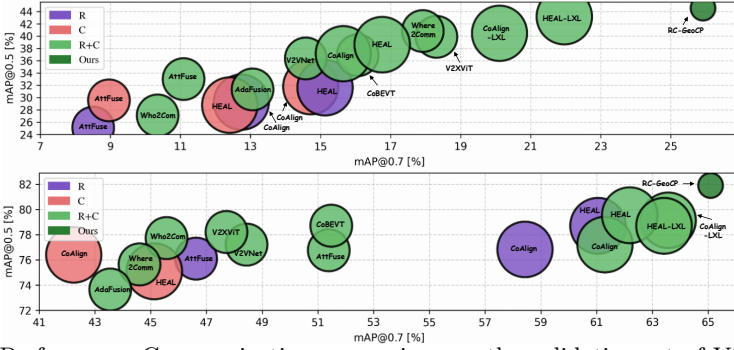


**Fig. 3:** Performance-Communication comparison on the validation set of V2X-Radar [50] (up) and V2X-R [13] (down) datasets, respectively. The communication cost are represented by the diameter of the blobs.

this through a Consensus-Driven Assembler, where radar-derived geometric consensus provides a shared physical reference to regulate fusion.

Specifically, each agent first predicts a radar-based geometric reliability map from its radar feature using a learnable mapping followed by sigmoid activation. The reliability scores are then aligned to the ego frame through spatial transformation  $\mathcal{T}_{j \rightarrow i}(\cdot)$ , providing geometry-aware confidence at each location without transmitting radar features. The aligned geometric consensus across agents is denoted by  $\mathbf{G}_{i,j}^{(l)}(p)$ , which represents the ego-aligned geometric reliability of agent  $j$  at BEV location  $p$ , normalized across all participating agents.

We leverage this geometric consensus to drive token aggregation by injecting geometry information into the attention logits. For each neighboring agent  $j$ , we gather its transmitted token set to ego  $i$  at scale  $l$ , including the selected ego-demand tokens and one agent-wise token, and stack them as

$$\mathbf{X}_{j \rightarrow i}^{(l)} = [\mathbf{t}_{j,1}^{(l)}, \dots, \mathbf{t}_{j,M}^{(l)}]^\top \in \mathbb{R}^{M \times C}, \quad M = |\Omega_{i,j}^{(l)}| + 1, \quad (11)$$

where  $\{\mathbf{t}_{j,m}^{(l)}\}_{m=1}^{M-1}$  are the selected tokens indexed by  $\Omega_{i,j}^{(l)}$  and  $\mathbf{t}_{j,M}^{(l)}$  is the agent-wise token. We then compute content-based attention logits as

$$\mathbf{A}_{j \rightarrow i}^{(l)} = \frac{\mathbf{X}_{j \rightarrow i}^{(l)} (\mathbf{X}_{j \rightarrow i}^{(l)})^\top}{\sqrt{C}}, \quad (12)$$

which models pairwise similarity among the transmitted tokens from agent  $j$ .

To inject geometric consistency, we associate each selected token with the ego-aligned geometric consensus  $\mathbf{G}_{i,j}^{(l)}(p)$  at its corresponding BEV location  $p \in \Omega_{i,j}^{(l)}$ , and use it as a logit prior. The attention matrix is obtained by

$$\mathbf{A}_{j \rightarrow i}^{(l)} = \text{Softmax} \left( \mathbf{A}_{j \rightarrow i}^{(l)} + \log \mathbf{g}_{j \rightarrow i}^{(l)} \right), \quad (13)$$

where  $\mathbf{g}_{j \rightarrow i}^{(l)} \in \mathbb{R}^M$  stacks the geometric priors of the  $M$  tokens (with the last entry corresponding to the agent-wise token), and the softmax is applied over

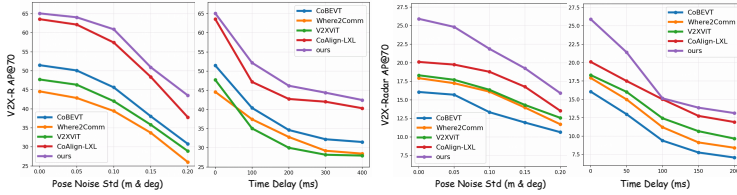


**Fig. 4:** Comparison of performance with baselines on the pose error and time delay setting on the validation set of V2X-Radar [50] and V2X-R [13] datasets, respectively.

the token dimension. The re-aggregated token set is then computed as  $\hat{\mathbf{X}}_{j \rightarrow i}^{(l)} = \mathbf{A}_{j \rightarrow i}^{(l)} \mathbf{X}_{j \rightarrow i}^{(l)}$ . Finally, at scale  $l$ , the re-aggregated tokens are unpacked to the BEV grid to form the collaborative representation, and fused through ego demand map introduced in 3.4 to get  $\mathbf{F}^{\text{collab},(l)}$ . As a result, multi-scale collaborative features can be fused to obtain  $\mathbf{F}_i^{\text{collab}}$ , which is expressed as  $\mathbf{F}_i^{\text{collab}} = \mathcal{F}(\{\mathbf{F}_i^{\text{collab},(l)}\}_{l=1}^L)$ , where  $\mathcal{F}(\cdot)$  denotes a lightweight multi-scale fusion operator.

This design allows geometric consensus to regulate both normalized fusion weights and content-based attention, yielding physically grounded and spatially consistent multi-agent aggregation. By regulating aggregation with radar-based geometric consensus, CDA enforces physically grounded and spatially consistent multi-agent perception without additional communication overhead.

## 4 Experiment

### 4.1 Implementation Details

**Datasets and Evaluation Metrics.** We evaluate models on the V2X-Radar [50] and V2X-R [13] datasets following their official protocols. The V2X-R dataset is a simulated dataset generated using the CARLA simulator, while V2X-Radar consists of real-world data collected. For V2X-R, we use 8,084 / 829 / 3,166 frames for training, validation, and testing, respectively, with 2–5 agents per frame, and report results within  $x \in [0.0, 140.0]$  m and  $y \in [-40.0, 40.0]$  m in bird’s-eye-view under the camera field of view constraint. For V2X-Radar, we use 5,367 training frames and 922 validation frames, and evaluate all results on the validation set within  $x, y \in [-102.4, 102.4]$  m relative to the ego vehicle, considering only objects within the valid radar sensing range. To provide a standardized metric for bandwidth efficiency, we define one communication base unit as  $64 \times 64 \times 256 \times 4$  bytes. The communication cost for each method is reported as the total transmitted bytes normalized by this base unit. Other configurations and evaluation settings follow the original implementations.

**Network Settings and Training details.** For feature extraction, we use RadarPillarNet [55] for 4D radar point clouds and EfficientNet [36] for image features. All models are trained on 4 NVIDIA H100 GPUs using the Adam [25] optimizer with a learning rate of  $1 \times 10^{-3}$ ,  $\epsilon = 1 \times 10^{-10}$ , and a weight decay of  $1 \times 10^{-4}$ . We adopt a CosineAnnealing learning rate schedule with linear warm-up for 500 iterations, a warm-up ratio of 0.1, and a minimum learning rate ratio of  $1 \times 10^{-5}$ . Other network configurations and training settings follow the original implementations. See supplementary materials for more details.

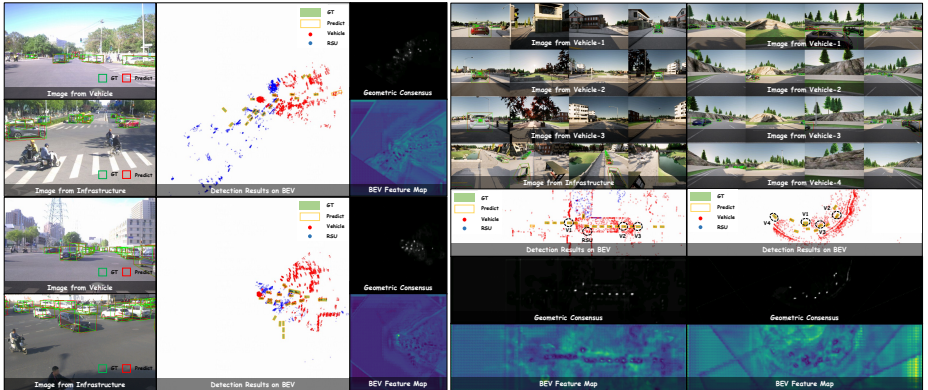


**Fig. 5:** Visualization results on the (a) V2X-Radar and (b) V2X-R. Each figure corresponds to a frame. We have annotated the bounding box. Zoom in for better view.

## 4.2 Quantitative Results

**Comparison with collaborative perception models.** Table 1 reports results on V2X-Radar [50] and V2X-R [13] under a unified multi-modal setting. On the V2X-Radar val split, RC-GeoCP delivers 44.55% AP@0.5 and 25.92% AP@0.7, surpassing the strongest prior methods, Where2comm [11] and V2XViT [47], by 3.72% and 7.61%, respectively. Notably, the performance gap widens under the stricter AP@0.7 criterion, highlighting a marked improvement in localization accuracy and geometric consistency. A similar trend is observed on the V2X-Radar test set, where RC-GeoCP registers 42.61% AP@0.5 and 18.77% AP@0.7, exceeding the best competing approaches (V2XViT [47] at AP@0.5 and CoAlign [27] at AP@0.7) by 7.80% and 6.42%, respectively. These consistent margins across validation and test splits indicate strong generalization capability.

On the V2X-R validation benchmark, RC-GeoCP achieves 81.90% AP@0.5 and 65.09% AP@0.7, outperforming the most competitive baseline HEAL by 2.36% and 2.90%, respectively. We observe that the absolute performance gains on V2X-R are more moderate compared to those on V2X-Radar. This stems from the inherent characteristics of the datasets: V2X-R is a simulated environment providing multi-view images for each agent, which naturally mitigates the "depth ambiguity" and spatial dispersion issues typical of monocular vision. In contrast, on the single-image real-world V2X-Radar dataset, our radar-anchored geometric grounding serves as a crucial corrective mechanism where visual semantics alone are structurally insufficient. Despite the richer visual coverage in V2X-R, RC-GeoCP still establishes a new state-of-the-art performance. Notably, these improvements are achieved with a communication cost of only 2.39, which is lower than all competing methods. This represents a bandwidth reduction of over 40% relative to standard 4.00-communication baselines and nearly 66% compared to high-overhead approaches like CoAlign and HEAL, demonstrating a superior balance between perception accuracy and communication efficiency.

Overall, RC-GeoCP establishes a new state of the art across all benchmarks while simultaneously achieving superior communication efficiency, validating the

**Table 2:** Cooperative perception on V2X-Radar [50] dataset. Agent denotes the cooperative fusion strategy across agents, independent of modality. In the modality column, R denotes 4D Radar while C denotes camera.

Agent	M	Fusion Strategy	AP@0.7 $\uparrow$				AP@0.5 $\uparrow$			
			Overall	0-30	30-50	50-100	Overall	0-30	30-50	50-100
AttFuse [48]	C	BEVDepth [19]	8.96	16.56	3.14	0.10	29.55	51.00	9.90	0.36
	R	RadarPillarNet [55]	8.51	14.76	3.14	0.23	25.11	38.02	15.98	2.35
	R+C	BEVFusion [24]	11.09	20.41	3.41	0.03	33.01	55.62	16.07	0.42
	R+C	RCFusion [55]	11.48	20.34	3.56	0.14	33.26	54.52	16.96	1.97
	R+C	LXL [43]	11.75	21.61	2.39	0.29	33.46	55.77	16.57	2.53
R+C	RC-GeoCP	14.36	23.85	7.63	0.04	35.02	56.25	21.91	1.07	
CoAlign [27]	C	BEVDepth [19]	14.72	25.93	2.55	0.01	31.77	52.83	10.11	0.14
	R	RadarPillarNet [55]	12.74	22.32	3.64	0.15	29.26	44.28	16.96	1.87
	R+C	BEVFusion [24]	15.65	26.81	3.24	0.99	37.14	57.89	18.96	2.78
	R+C	RCFusion [55]	16.26	28.77	4.25	0.40	37.60	57.91	19.90	2.64
	R+C	LXL [43]	20.11	33.85	4.45	0.11	40.46	61.60	19.02	2.21
R+C	RC-GeoCP	24.87	40.53	8.75	0.60	44.77	65.60	28.68	3.91	
HEAL [26]	C	BEVDepth [19]	12.41	22.94	2.21	0.01	28.78	53.39	7.36	0.07
	R	RadarPillarNet [55]	15.13	24.69	5.93	0.38	31.61	46.87	19.32	1.94
	R+C	BEVFusion [24]	16.76	27.59	6.68	0.27	38.61	58.74	23.49	2.66
	R+C	RCFusion [55]	17.47	29.48	6.82	0.88	38.89	56.62	25.48	2.37
	R+C	LXL [43]	21.96	36.37	6.34	0.40	43.17	64.02	24.92	2.52
R+C	RC-GeoCP	26.30	43.94	9.27	0.31	46.17	68.13	29.30	2.48	

effectiveness of consensus-guided token aggregation for radar-camera CP. The overall performance comparisons are illustrated in Figure 3.

**Comparison with radar-camera models.** Tables 2 and 3 present detailed comparisons with representative radar-camera collaborative perception models under different radar-camera fusion strategies, including camera-only BEVDepth [19], radar-only RadarPillarNet [55], and radar-camera baselines including BEVFusion [24], RCFusion [55], and LXL [43]. To ensure fairness, RC-GeoCP is implemented on top of the official codebase of each CP framework.

On V2X-Radar [50], RC-GeoCP consistently outperforms all radar-camera baselines across cooperative frameworks. Under AttFuse [48], the strongest prior radar-camera model LXL achieves 11.75% mAP at IoU 0.7, whereas RC-GeoCP raises it to 14.36%, yielding a 2.61% gain. The improvement becomes more substantial under stronger cooperative backbones: within CoAlign [27], AP@0.7 increases from 20.11% to 24.87%, and under HEAL [26], from 21.96% to 26.30%. These consistent margins indicate that the proposed geometric consensus mechanism complements, rather than replaces, existing radar-camera fusion strategies. The advantage is particularly pronounced in the medium-distance range between 30 and 50 meters. For instance, under CoAlign at IoU 0.7, performance improves from 4.45% to 8.75%, nearly doubling the accuracy. This suggests that radar-anchored geometric consensus effectively mitigates depth ambiguity and spatial dispersion in scenarios where camera features are less reliable.

On V2X-R [13], similar trends are observed in both synchronous and asynchronous settings. Under CoAlign, synchronous AP@0.7 improves from 63.57% to 67.40%, while asynchronous performance increases from 54.82% to 58.99%. The consistent gains across temporal settings indicate that consensus-guided token aggregation enhances not only spatial alignment but also robustness to temporal misalignment. Overall, the results demonstrate that injecting radar-derived geometric consensus into token-level aggregation provides systematic improve-

**Table 3:** Cooperative perception on V2X-R [13] dataset. Asynchronous denotes a 100 ms delay, which is simulated by retrieving samples from the preceding timestamp.

Agent	M	Extractor	Synchronous AP@0.7 $\uparrow$				Asynchronous AP@0.7 $\uparrow$			
			Overall	0-30	30-50	50-100	Overall	0-30	30-50	50-100
AttFuse [48]	C	BEVDepth [19]	31.18	43.29	26.04	23.38	22.20	36.41	16.32	11.80
	R	RadarPillarNet [55]	46.63	66.10	44.36	28.36	41.62	59.31	41.97	22.05
	R+C	BEVFusion [24]	51.39	70.84	51.31	34.76	42.77	62.77	36.47	27.85
	R+C	RCFusion [55]	52.99	72.90	52.16	34.80	43.68	64.61	41.94	25.08
	R+C	LXL [43]	52.80	72.21	52.62	34.67	43.75	63.47	40.39	26.35
R+C	RC-GeoCP	54.19	73.29	53.11	35.28	44.12	64.99	42.53	26.01	
CoAlign [27]	C	BEVDepth [19]	42.24	56.40	42.43	28.74	37.87	53.18	35.36	26.05
	R	RadarPillarNet [55]	58.43	76.83	62.64	34.98	50.23	70.17	53.13	26.25
	R+C	BEVFusion [24]	61.30	80.35	65.22	33.02	54.63	76.89	51.22	36.01
	R+C	RCFusion [55]	60.22	78.69	64.08	40.10	56.07	79.42	55.33	35.19
	R+C	LXL [43]	63.57	82.63	66.51	45.11	54.82	77.82	54.26	33.18
R+C	RC-GeoCP	67.40	86.27	69.51	48.95	58.99	81.91	57.65	38.09	
HEAL [26]	C	BEVDepth [19]	45.13	59.09	43.77	34.45	33.94	53.74	29.03	16.65
	R	RadarPillarNet [55]	61.05	81.70	64.21	35.19	50.11	69.62	54.22	25.24
	R+C	BEVFusion [24]	62.19	83.94	65.97	35.65	51.45	77.16	50.25	26.96
	R+C	RCFusion [55]	62.77	82.47	68.93	38.25	57.36	80.17	58.51	32.81
	R+C	LXL [43]	63.42	83.29	70.75	39.84	48.19	71.25	48.15	23.18
R+C	RC-GeoCP	65.66	87.64	70.15	39.16	58.65	81.87	60.02	34.21	

**Table 4:** Overall ablation study of different proposed modules on the validation set of V2X-R and V2X-Radar datasets.

Base	GSR	CDA	UAC	V2X-R $\uparrow$		V2X-Radar $\uparrow$	
				AP@0.7	AP@0.5	AP@0.7	AP@0.5
✓				61.30	76.21	16.76	38.61
✓	✓			64.99	78.14	23.81	43.12
✓		✓		62.84	77.90	22.78	41.89
✓	✓	✓		67.40	79.85	26.30	46.17
✓	✓	✓	✓	65.09	81.90	25.92	44.55

**Table 5:** Hyperparameter and performance trade-off analysis of UAC transmission ratios.

Comm. Ratio $\downarrow$	V2X-R $\uparrow$			
	AP@0.7	AP@0.5	AP@0.7	AP@0.5
~25%	60.95	78.34	25.88	44.50
~50%	62.88	79.83	25.93	44.54
~60%	63.54	80.12	25.91	44.49
~75%	65.09	81.90	25.92	44.55
~100%	67.40	79.85	26.30	46.17

ments over conventional radar-camera fusion models, especially in geometrically challenging and temporally inconsistent scenarios.

**Robustness analysis.** In real-world deployment, pose estimation errors and communication latency are unavoidable, particularly in heterogeneous collaborative settings. To evaluate the practical robustness of RC-GeoCP, we further conduct experiments under simulated pose perturbations and temporal asynchrony. As illustrated in Figure 4, RC-GeoCP consistently demonstrates stronger robustness to both pose noise and temporal misalignment compared to state-of-the-art methods, maintaining more stable detection performance under increasing disturbance levels. Detailed analysis of the ablation results is provided in the supplementary material.

### 4.3 Visualization Results

Figure 5 presents qualitative results on V2X-Radar [50] and V2X-R [13]. V2X-Radar adopts a single-image-per-agent setting, while V2X-R provides multi-view images for each vehicle, resulting in richer visual coverage. In both datasets, image-space predictions closely align with ground truth across vehicle and infrastructure views. In the BEV perspective, detections from multiple agents are spatially consistent and well aligned, demonstrating effective cross-agent fusion. The geometric consensus maps exhibit structured activations concentrated around object regions, indicating reliable radar-guided spatial anchoring. Correspondingly, the BEV feature maps show enhanced object-focused responses after

**Table 6:** Geometry consensus/demand map for agent fusion impact on fusion accuracy.

CDA	V2X-R $\uparrow$		V2X-Radar $\uparrow$	
	AP@0.7	AP@0.5	AP@0.7	AP@0.5
w/o consensus	65.65	79.81	24.97	44.38
w/ consensus	67.40	79.85	26.30	46.17
w/o demand map	64.19	76.20	24.74	43.40

**Table 7:** Performance with and without agent-wise tokens

Agent-wise Token	V2X-R $\uparrow$		V2X-Radar $\uparrow$	
	AP@0.7	AP@0.5	AP@0.7	AP@0.5
w/o	65.90	78.96	24.78	44.08
w/	67.40	79.85	26.30	46.17
pooling	67.01	80.12	25.92	44.55

rectification and aggregation, demonstrating effectiveness of RC-GeoCP. More visualization result will be presented in supplementary materials.

#### 4.4 Ablation Study

Overall Effectiveness and Communication Efficiency. As shown in Table 4, starting from the Base model, adding GSR yields a substantial 7.05% absolute improvement in AP@0.7 on V2X-Radar [50], confirming that radar-anchored grounding is essential to counteract depth-semantic diffusion. The synergy of GSR and CDA achieves peak performance, 26.30% AP@0.7 on V2X-Radar and 67.40% on V2X-R [13]. Building on this foundation, Table 5 analyzes the trade-off between communication ratio and accuracy. Increasing the transmission ratio from 25% to 75% consistently improves performance on V2X-R, while dense 100% transmission offers diminishing returns. Notably, performance on V2X-Radar remains remarkably stable across various ratios, demonstrating that UAC successfully preserves critical geometric information even under high sparsity of realistic radar data. Overall, RC-GeoCP achieves an optimal balance between local computational refinement and global communication efficiency.

To further decompose the source of these gains, Table 6 investigates the internal mechanisms of the Consensus-Driven Assembler. Utilizing radar-based geometric consensus as a shared physical reference provides a 1.33% AP@0.7 gain on V2X-Radar, ensuring the alignment of semantically diffuse features. Simultaneously, the demand map enables the system to prioritize tokens that fill specific perceptual gaps, ensuring cross-agent structural consistency. Finally, to mitigate information loss during sparse top-K selection, we evaluate the agent-wise token in Table 7 for analyzing global context preservation. Compared to discarding residual features entirely, our learnable token provides a significant +1.52% AP@0.7 boost on V2X-Radar. This context summarizer ensures that even under a reduced communication cost of 2.39 units, RC-GeoCP preserves essential environmental context beyond local observations, outperforming traditional pooling strategies.

## 5 Conclusions

This work presents RC-GeoCP, which introduces the first framework for 4D radar-camera collaborative perception. By utilizing the geometric stability of radar, GSR grounds camera semantics in physical space, while UAC and CDA facilitate efficient information selection and multi-agent fusion. This geometry-driven design establishes an efficient pipeline that achieves robust perception with minimal communication cost. Extensive evaluations on V2X-Radar and V2X-R benchmarks demonstrate superior performance-bandwidth trade-offs. This

work underscores the significance of radar-camera collaboration and provides a principled path toward scalable perception systems.

*Discussion.* Although evaluated on homogeneous sensors, RC-GeoCP utilizes discrete radar anchors to ensure robustness against varying radar sensors. Future research will investigate scalability within heterogeneous V2X ecosystems.

## References

1. Bai, X., Cheng, J., Wang, S., Luo, Y., Zheng, L., Zhang, X., Cao, S.Y., Shen, H.L.: SD4R: Sparse-to-Dense Learning for 3D Object Detection with 4D Radar. arXiv preprint arXiv:2602.20653 (2026) [4](#)
2. Bai, X., Yang, Q., Zhou, Z., Zhang, F., Wu, Z., Cao, S.Y., Zheng, L., Yu, B., Wang, F., Bai, J., et al.: LGDD: Local-Global Synergistic Dual-Branch 3D Object Detection Using 4D Radar. In: IEEE/RSJ International Conference on Intelligent Robots and Systems (IROS). pp. 13318–13325. IEEE (2025) [4](#)
3. Bai, X., Yu, Z., Zheng, L., Zhang, X., Zhou, Z., Zhang, X., Wang, F., Bai, J., Shen, H.L.: SGMet3D: Semantics and Geometry Fusion for 3D Object Detection Using 4D Radar and Camera. IEEE Robotics and Automation Letters pp. 1–8 (2024). <https://doi.org/10.1109/LRA.2024.3513041> [4](#)
4. Bai, X., Zhou, C., Zheng, L., Cao, S.Y., Liu, J., Zhang, X., Li, Y., Zhang, Z., Shen, H.L.: RaGS: Unleashing 3D Gaussian Splatting from 4D Radar and Monocular Cues for 3D Object Detection. In: IEEE/CVF Conference on Computer Vision and Pattern Recognition (2026) [4](#)
5. Chen, G., Zhang, C., Lv, P., Xie, X.: CoRA: A Collaborative Robust Architecture with Hybrid Fusion for Efficient Perception. arXiv preprint arXiv:2512.13191 (2025) [2](#)
6. Chen, Q., Ma, X., Tang, S., Guo, J., Yang, Q., Fu, S.: F-Cooper: Feature based Cooperative Perception for Autonomous Vehicle Edge Computing System Using 3D Point Clouds. In: ACM/IEEE Symposium on Edge Computing. pp. 88–100 (2019) [1](#), [2](#)
7. Dreissig, M., Scheuble, D., Piewak, F., Boedecker, J.: Survey on LiDAR Perception in Adverse Weather Conditions. In: IEEE Intelligent Vehicles Symposium. pp. 1–8 (2023) [2](#)
8. Fan, L., Wang, J., Chang, Y., Li, Y., Wang, Y., Cao, D.: 4D mmWave Radar for Autonomous Driving Perception: A Comprehensive Survey. IEEE Transactions on Intelligent Vehicles **9**(4), 4606–4620 (2024). <https://doi.org/10.1109/TIV.2024.3380244> [2](#)
9. Gu, J., Zhang, J., Zhang, M., Meng, W., Xu, S., Zhang, J., Zhang, X.: FeaCo: Reaching Robust Feature-Level Consensus in Noisy Pose Conditions. In: ACM International Conference on Multimedia. pp. 3628–3636 (2023) [2](#), [3](#)
10. Hong, S., Liu, Y., Li, Z., Li, S., He, Y.: Multi-agent Collaborative Perception via Motion-aware Robust Communication Network. In: IEEE/CVF Conference on Computer Vision and Pattern Recognition. pp. 15301–15310 (2024) [2](#)
11. Hu, Y., Fang, S., Lei, Z., Zhong, Y., Chen, S.: Where2comm: Communication-Efficient Collaborative Perception via Spatial Confidence Maps. Advances in neural information processing systems **35**, 4874–4886 (2022) [1](#), [2](#), [3](#), [8](#), [11](#)
12. Hu, Y., Peng, J., Liu, S., Ge, J., Liu, S., Chen, S.: Communication-Efficient Collaborative Perception via Information Filling with Codebook. In: IEEE/CVF Conference on Computer Vision and Pattern Recognition. pp. 15481–15490 (2024) [1](#)

13. Huang, X., Wang, J., Xia, Q., Chen, S., Yang, B., Li, X., Wang, C., Wen, C.: V2X-R: Cooperative LiDAR-4D Radar Fusion with Denoising Diffusion for 3D Object Detection. In: IEEE/CVF conference on Computer Vision and Pattern Recognition. pp. 27390–27400 (2025) [2](#), [3](#), [4](#), [8](#), [9](#), [10](#), [11](#), [12](#), [13](#), [14](#)
14. Kim, Y., Kim, S., Choi, J.W., Kum, D.: CRAFT: Camera-Radar 3D Object Detection with Spatio-Contextual Fusion Transformer. In: AAAI Conference on Artificial Intelligence. vol. 37, pp. 1160–1168 (2023) [2](#), [4](#)
15. Kim, Y., Shin, J., Kim, S., Lee, I.J., Choi, J.W., Kum, D.: CRN: Camera Radar Net for Accurate, Robust, Efficient 3D Perception. In: IEEE/CVF International Conference on Computer Vision. pp. 17615–17626 (2023) [4](#)
16. Lai, H., Yin, P., Scherer, S.: AdaFusion: Visual-LiDAR Fusion with Adaptive Weights for Place Recognition. *IEEE Robotics and Automation Letters* **7**(4), 12038–12045 (2022) [8](#)
17. Li, X., Di, H., Li, J., Liu, F., Liang, W.: M3Detection: Multi-Frame Multi-Level Feature Fusion for Multi-Modal 3D Object Detection with Camera and 4D Imaging Radar. *arXiv preprint arXiv:2510.27166* (2025) [4](#)
18. Li, Y., Ren, S., Wu, P., Chen, S., Feng, C., Zhang, W.: Learning Distilled Collaboration Graph for Multi-Agent Perception. *Advances in Neural Information Processing Systems* **34**, 29541–29552 (2021) [1](#), [2](#)
19. Li, Y., Ge, Z., Yu, G., Yang, J., Wang, Z., Shi, Y., Sun, J., Li, Z.: BEVDepth: Acquisition of Reliable Depth for Multi-View 3D Object Detection. In: AAAI Conference on Artificial Intelligence. pp. 1477–1485 (2023) [2](#), [12](#), [13](#)
20. Li, Z., Wang, W., Li, H., Xie, E., Sima, C., Lu, T., Qiao, Y., Dai, J.: BEVFormer: Learning Bird’s-Eye-View Representation from Multi-camera Images via Spatiotemporal Transformers. In: European Conference on Computer Vision. pp. 1–18 (2022) [2](#)
21. Lin, Z., Liu, Z., Xia, Z., Wang, X., Wang, Y., Qi, S., Dong, Y., Dong, N., Zhang, L., Zhu, C.: RCBEVDet: Radar-camera Fusion in Bird’s Eye View for 3D Object Detection. In: IEEE/CVF conference on Computer Vision and Pattern Recognition. pp. 14928–14937 (2024) [4](#)
22. Liu, Y.C., Tian, J., Glaser, N., Kira, Z.: When2com: Multi-Agent Perception via Communication Graph Grouping. In: IEEE/CVF Conference on computer vision and pattern recognition. pp. 4106–4115 (2020) [2](#)
23. Liu, Y.C., Tian, J., Ma, C.Y., Glaser, N., Kuo, C.W., Kira, Z.: Who2com: Collaborative Perception via Learnable Handshake Communication. In: IEEE International Conference on Robotics and Automation (ICRA). pp. 6876–6883. *IEEE* (2020) [3](#), [8](#)
24. Liu, Z., Tang, H., Amini, A., Yang, X., Mao, H., Rus, D.L., Han, S.: BEVFusion: Multi-Task Multi-Sensor Fusion with Unified Bird’s-Eye View Representation. In: IEEE International Conference on Robotics and Automation. pp. 2774–2781 (2023) [12](#), [13](#)
25. Loshchilov, I., Hutter, F.: Decoupled Weight Decay Regularization. *arXiv preprint arXiv:1711.05101* (2017) [10](#)
26. Lu, Y., Hu, Y., Zhong, Y., Wang, D., Wang, Y., Chen, S.: An Extensible Framework for Open Heterogeneous Collaborative Perception. In: International Conference on Learning Representations (2024) [8](#), [12](#), [13](#)
27. Lu, Y., Li, Q., Liu, B., Dianati, M., Feng, C., Chen, S., Wang, Y.: Robust Collaborative 3D Object Detection in Presence of Pose Errors. In: IEEE International Conference on Robotics and Automation. pp. 4812–4818. *IEEE* (2023) [3](#), [4](#), [8](#), [11](#), [12](#), [13](#)

28. Mohammed, A.S., Amamou, A., Ayevide, F.K., Kelouwani, S., Agbossou, K., Zioui, N.: The Perception System of Intelligent Ground Vehicles in All Weather Conditions: A Systematic Literature Review. *Sensors* **20**(22), 6532 (2020) [2](#)
29. Nabati, R., Qi, H.: CenterFusion: Center-based Radar and Camera Fusion for 3D Object Detection. In: *IEEE/CVF Winter Conference on Applications of Computer Vision*. pp. 1527–1536 (2021) [2](#), [4](#)
30. Park, J., Xu, C., Yang, S., Keutzer, K., Kitani, K., Tomizuka, M., Zhan, W.: Time Will Tell: New Outlooks and A Baseline for Temporal Multi-View 3D Object Detection. *International Conference on Learning Representations* (2022) [2](#)
31. Philion, J., Fidler, S.: Lift, Splat, Shoot: Encoding Images from Arbitrary Camera Rigs by Implicitly Unprojecting to 3D. In: *European Conference on Computer Vision*. pp. 194–210 (2020) [2](#), [4](#)
32. Scheiner, N., Kraus, F., Appenrodt, N., Dickmann, J., Sick, B.: Object Detection for Automotive Radar Point Clouds – A Comparison. *AI Perspectives* **3**(1), 6 (2021) [2](#)
33. Shenkut, D., Bhagavatula, V.: FocalComm: Hard Instance-Aware Multi-Agent Perception. *arXiv preprint arXiv:2512.13982* (2025) [3](#)
34. Song, Z., Xie, T., Zhang, H., Liu, J., Wen, F., Li, J.: A Spatial Calibration Method for Robust Cooperative Perception. *IEEE Robotics and Automation Letters* **9**(5), 4011–4018 (2024) [3](#)
35. Song, Z., Yang, L., Wen, F., Li, J.: TraF-Align: Trajectory-aware Feature Alignment for Asynchronous Multi-agent Perception. In: *IEEE/CVF Conference on Computer Vision and Pattern Recognition*. pp. 12048–12057 (2025) [4](#)
36. Tan, M., Le, Q.: EfficientNet: Rethinking Model Scaling for Convolutional Neural Networks. In: *International Conference on Machine Learning*. pp. 6105–6114. PMLR (2019) [10](#)
37. Tang, Z., Liu, Y., Sun, Y., Gao, Y., Chen, J., Xu, R., Liu, S.: CoST: Efficient Collaborative Perception From Unified Spatiotemporal Perspective. In: *IEEE/CVF International Conference on Computer Vision*. pp. 1120–1129 (2025) [1](#)
38. Wang, T., Lu, F., Zheng, Z., Chen, G., Jiang, C.: RCDN: Towards Robust Camera-Insensitivity Collaborative Perception via Dynamic Feature-based 3D Neural Modeling. *Advances in Neural Information Processing Systems* **37**, 22350–22369 (2024) [2](#)
39. Wang, T.H., Manivasagam, S., Liang, M., Yang, B., Zeng, W., Urtasun, R.: V2VNet: Vehicle-to-Vehicle Communication for Joint Perception and Prediction. In: *European conference on computer vision*. pp. 605–621. Springer (2020) [1](#), [2](#), [3](#), [8](#)
40. Wang, Y., Chen, Y., Liao, X., Fan, L., Zhang, Z.: Panoocc: Unified occupancy representation for camera-based 3d panoptic segmentation. In: *IEEE/CVF conference on Computer Vision and Pattern Recognition*. pp. 17158–17168 (2024) [2](#)
41. Wu, Y., Xiao, L., Liu, J., Jiang, G., Xia, X.: MLF-4DRCNet: Multi-Level Fusion with 4D Radar and Camera for 3D Object Detection in Autonomous Driving. *arXiv preprint arXiv:2509.18613* (2025) [4](#)
42. Xiang, H., Xu, R., Ma, J.: HM-ViT: Hetero-modal Vehicle-to-Vehicle Cooperative Perception with Vision Transformer. In: *Proceedings of the IEEE/CVF international conference on computer vision*. pp. 284–295 (2023) [1](#), [2](#)
43. Xiong, W., Liu, J., Huang, T., Han, Q.L., Xia, Y., Zhu, B.: LXL: LiDAR Excluded Lean 3D Object Detection with 4D Imaging Radar and Camera Fusion. *IEEE Transactions on Intelligent Vehicles* **9**(1), 79–92 (2024). <https://doi.org/10.1109/TIV.2023.3321240> [2](#), [4](#), [12](#), [13](#)

44. Xiong, W., Zou, Z., Zhao, Q., He, F., Zhu, B.: LXLv2: Enhanced LiDAR Excluded Lean 3D Object Detection with Fusion of 4D Radar and Camera. *IEEE Robotics and Automation Letters (RAL)* (2025) [2](#)
45. Xu, R., Tu, Z., Xiang, H., Shao, W., Zhou, B., Ma, J.: CoBEVT: Cooperative Bird's Eye View Semantic Segmentation with Sparse Transformers. In: *Annual Conference on Robot Learning*. p. 989–1000 (2023) [1](#), [2](#), [3](#), [8](#)
46. Xu, R., Xia, X., Li, J., Li, H., Zhang, S., Tu, Z., Meng, Z., Xiang, H., Dong, X., Song, R., et al.: V2V4Real: A Real-world Large-scale Dataset for Vehicle-to-Vehicle Cooperative Perception. In: *Proceedings of the IEEE/CVF conference on computer vision and pattern recognition*. pp. 13712–13722 (2023) [1](#)
47. Xu, R., Xiang, H., Tu, Z., Xia, X., Yang, M.H., Ma, J.: V2X-ViT: Vehicle-to-Everything Cooperative Perception with Vision Transformer. In: *European conference on computer vision*. pp. 107–124. Springer (2022) [1](#), [2](#), [3](#), [8](#), [11](#)
48. Xu, R., Xiang, H., Xia, X., Han, X., Li, J., Ma, J.: OPV2V: An Open Benchmark Dataset and Fusion Pipeline for Perception with Vehicle-to-Vehicle Communication. In: *International Conference on Robotics and Automation*. pp. 2583–2589. IEEE (2022) [1](#), [8](#), [12](#), [13](#)
49. Yang, K., Yang, D., Li, K., Xiao, D., Shao, Z., Sun, P., Song, L.: Align before Collaborate: Mitigating Feature Misalignment for Robust Multi-Agent Perception. In: *European Conference on Computer Vision*. pp. 282–299. Springer (2024) [2](#)
50. Yang, L., Zhang, X., Li, J., Wang, C., Ma, J., Song, Z., Zhao, T., Song, Z., Wang, L., Zhou, M., et al.: V2X-Radar: A Multi-modal Dataset with 4D Radar for Cooperative Perception. *arXiv preprint arXiv:2411.10962* (2024) [2](#), [3](#), [8](#), [9](#), [10](#), [11](#), [12](#), [13](#), [14](#)
51. Yazgan, M., Wu, Q., Hamdard, I., Li, S., Zoellner, J.M.: SlimComm: Doppler-Guided Sparse Queries for Bandwidth-Efficient Cooperative 3D Perception. In: *IEEE/CVF International Conference on Computer Vision*. pp. 1782–1791 (2025) [1](#), [2](#), [3](#), [4](#)
52. Yu, H., Luo, Y., Shu, M., Huo, Y., Yang, Z., Shi, Y., Guo, Z., Li, H., Hu, X., Yuan, J., et al.: DAIR-V2X: A Large-Scale Dataset for Vehicle-Infrastructure Cooperative 3D Object Detection. In: *Proceedings of the IEEE/CVF conference on computer vision and pattern recognition*. pp. 21361–21370 (2022) [1](#)
53. Zhang, H., Wu, Y., Zhang, Z.: What2Keep: A Communication-Efficient Collaborative Perception Framework for 3D Detection via Keeping Valuable Information. *Computer Vision and Image Understanding* p. 104572 (2025) [2](#), [3](#)
54. Zhang, Y., Carballo, A., Yang, H., Takeda, K.: Perception and sensing for autonomous vehicles under adverse weather conditions: A survey Author links open overlay panel. *ISPRS Journal of Photogrammetry and Remote Sensing* **196**, 146–177 (2023) [2](#)
55. Zheng, L., Li, S., Tan, B., Yang, L., Chen, S., Huang, L., Bai, J., Zhu, X., Ma, Z.: RCFusion: Fusing 4-D Radar and Camera with Bird's-Eye View Features for 3-D Object Detection. *IEEE Transactions on Instrumentation and Measurement* **72**, 1–14 (2023) [10](#), [12](#), [13](#)
56. Zheng, L., Liu, J., Guan, R., Yang, L., Lu, S., Li, Y., Bai, X., Bai, J., Ma, Z., Shen, H.L., et al.: Doracamom: Joint 3D Detection and Occupancy Prediction with Multi-view 4D Radars and Cameras for Omnidirectional Perception. *IEEE Transactions on Circuits and Systems for Video Technology* (2026) [4](#)
57. Zheng, L., Yang, L., Lin, Q., Ai, W., Liu, M., Lu, S., Liu, J., Ren, H., Mo, J., Bai, X., et al.: OmniHD-Scenes: A Next-Generation Multimodal Dataset for Autonomous Driving. *arXiv preprint arXiv:2412.10734* (2024) [4](#)

58. Zhou, Z., Xiang, H., Zheng, Z., Zhao, S.Z., Lei, M., Zhang, Y., Cai, T., Liu, X., Liu, J., Bajji, M., et al.: V2XPnP: Vehicle-to-Everything Spatio-Temporal Fusion for Multi-Agent Perception and Prediction. In: IEEE/CVF International Conference on Computer Vision. pp. 25399–25409 (2025) [1](#)